Surface Review and Letters, 1850167 (8 pages)

DOI: 10.1142/S0218625X18501676

STUDIES ON STRUCTURAL, SURFACE MORPHOLOGICAL, OPTICAL, LUMINESCENCE AND UV PHOTODETECTION PROPERTIES OF SOL–GEL Mg-DOPED ZnO THIN FILMS

A. MAHROUG*,**, B. MARI†, M. MOLLAR†, I. BOUDJADAR‡, L. GUERBOUS§, A. HENNI¶ and N. SELMI‖

*Laboratory of Materials Physics and Its Applications, University of M'sila, M'sila 28000, Algeria

†Institut de Disseny per a la Fabricació i Producció Automatitzada, Departamento de Física Aplicada, Universitat Politècnica de València, Camí de Vera S/N, 46022 València, Spain

‡Ceramics Laboratory, Department of Physics, Mentouri University of Constantine, Constantine 25000, Algeria

§Laser Department, Nuclear Research Centre of Algiers (CRNA), 2 Building Frantz Fanon, B.P. 399, Algiers 16000, Algeria

¶Department of Biological Sciences, Kasdi Merbah University of Ouargla, Ouargla 30000, Algeria

‖Nuclear Research Centre of Birine, P. O. Box 180, Ain Oussera 17200, Djelfa, Algeria

**m_abdelhafid@yahoo.fr

Received 13 November 2017
Revised 18 January 2018
Accepted 26 January 2018
Published 19 March 2018

Undoped and magnesium-doped zinc oxide thin films were prepared by the sol–gel method. Results from X-ray diffraction indicated that the films exhibited a hexagonal wurtzite structure and were highly oriented along the *c*-axis. The intensity of the (002) diffraction peak increased with increasing the Mg doping concentration. Also, Mg doping inhibited the growth of crystallite size which decreased from 46 nm to 38 nm with doping concentration. Morphological studies by atomic force microscopy (AFM) indicated the uniform thin film growth and the decreasing of grain size and surface roughness with Mg doping. Optical analysis showed that the average transmittance of all films was above 90% in the visible range and Mg doping has significantly enhanced the bandgap energy of ZnO. Two Raman modes assigned to E_{2L} and E_{2H} for the ZnO wurtzite structure were observed for all films. UV emission peak and three defect emission peaks in the visible region were observed by photoluminescence measurements at room temperature. The intensity ratio of UV emission to the visible emission increased with the Mg concentration. Photocurrent measurements revealed that all films presented the photoresponses with *n*-type semiconducting behavior and their

**Corresponding author.

generated photocurrents were reduced by Mg doping. The prepared thin films of high quality with improved properties by Mg doping could be proposed to workers in the field of optoelectronic devices for using them as a strong candidate.

Keywords: Sol–gel processes; Mg-doped ZnO thin film; structural properties; optical properties; luminescence; photocurrent.

1. Introduction

Recently, ZnO as an *n*-type semiconductor, with a high exciton binding energy (60 meV) and a wide bandgap (3.37 eV),[1] has attracted great attention due to its potential applications in different electronic and optoelectronic fields such as ultraviolet (UV) photodetectors, light-emitting diodes (LEDs), laser diodes (LDs), transparent conducting electrodes, catalysts and gas sensors.[2–12] So, it is required that ZnO must possess improved electrical and optical properties for such applications. Doping of ZnO with group-II elements such as Mg will enhance its electrical and optical properties.[13–16] In addition, the incorporation of Mg^{2+} ion into zinc oxide lattice is easily feasible, due to similar ionic radii of Zn^{2+} (0.06 nm) and Mg^{2+} (0.057 nm).[12,13] This improves the crystallinity of ZnO without changing the wurtzite structure.[6,7,13,17,18] Furthermore, the properties of these nanostructures are dependent on surface morphology, particle size, orientation, crystalline structure and concentrations of intrinsic and extrinsic defects, which can be modified by Mg doping. For more improvement of electrical and optical properties, the ZnMgO films doped with other elements like Na and Al have been extensively studied,[3,19] for solar cell applications. Various deposition techniques have been used to prepare Mg-doped ZnO thin films, such as RF sputtering, molecular beam epitaxy (MBE), spray pyrolysis, hydrothermal and sol–gel technique.[3,7–9,13–16,19–22] Among these techniques, sol–gel method has a distinct advantage: simple, economic and easy to perform doping incorporation. The films with preferential *c*-axis orientation of zinc oxide can be easily obtained by the sol–gel process, where a good *c*-axis-oriented crystalline structure is desirable for different applications such as piezoelectric devices.

In recent years, zinc oxide nanostructures doped with magnesium have been extensively studied. Huang *et al.*[14] investigated the structural and optical properties of Mg-doped ZnO thin films deposited by sol–gel method. They reported that a secondary phase of MgO is evolved for the thin film with Mg:Zn = 0.08, and the root mean square (RMS) roughness, the optical bandgap and the resistivity of the ZnO thin films increase with increasing Mg concentration. Arshad *et al.*[23] synthesized the Mg-doped ZnO nanoparticles by a wet chemical route. They reported that the Mg doping inhibited the growth of particle size, increased the optical gap and enhanced the visible photoluminescence (PL) emission. In their study on the influence of Mg doping on the properties of ZnO films prepared by sputtering, Karthick and Vijayalakshmi[15] demonstrated that the blueshift in the PL emission for Mg:ZnO film might be the reason of the modulation of bandgap with suppression of defect center by Mg addition. They also reported that a significant change in surface morphology of the films was observed with Mg doping. In addition, Madahi *et al.*[24] reported that ZnO:Mg thin films showed excellent antibacterial activity, which was enhanced by doping with Mg. Besides, Chebil *et al.*[10] reported in their work on Mg-doped ZnO prepared by sol–gel that the preferential orientation along the *c*-axis disappeared in ZnMgO thin films, and the crystallite size, the optical bandgap and the surface roughness increased by Mg doping. Also, Mia *et al.*[25] demonstrated in their work on Mg-doped ZnO thin film of 200 nm thickness which was fabricated by sol–gel spin coating method, that the sharp absorption edge exhibited blueshifts and the crystallite size increased with the increase of Mg content. Similar results were reported by Rouchdi *et al.*,[26] Yu *et al.* and Chen *et al.* in their interesting studies[27–29] reported that the reduced graphene oxide/WS2/Mg-doped ZnO composites and graphene oxide/Mg-doped ZnO nanohybrid have outstanding photocatalytic and anti-bacterial activities.

Various issues show that the physical properties of ZnO thin films are influenced by deposition technique and their growth conditions. For example, in sol–gel technique, the solubility of the elements, morphology,

grain size, structural and the optical properties of thin films are influenced by the precursors and their initial concentrations, nature of the alcoholic solvent, stabilizer and their concentrations, temperature and time of the heat treatment, substrates and speeds. After adjusting these parameters, high-quality undoped and Mg-doped ZnO thin films were successfully deposited on glass substrates by the sol–gel method and a spin coating technique. The effect of doping with Mg on the structure, surface morphologies, optical and photoelectrochemical properties of the thin films was investigated, and the obtained results of all thin films were compared with other experimental ones. Finally, we suggested a view depicting the energy band diagram and the origin of different emission peaks in the UV and visible regions. The change in optical properties was discussed from the point of view of the structural change of thin films and concentration defects induced by magnesium doping.

2. Experimental Details

Mg-doped ZnO thin films were prepared on glass substrates, using sol–gel spin coating technique. Figure 1 shows the flowchart of sol–gel process for preparing Mg-doped ZnO thin films. Magnesium chloride hexahydrate ($MgCl_2 \cdot 6H_2O$; 0, 1, 3, 5 and 7 mol.%), zinc acetate dihydrate ($Zn(CH_3COO)_2 \cdot 2H_2O$) with 0.6 mol/L for undoped ZnO, isopropanol and monoethanolamine (MEA) were used as the precursors, solvent and stabilizer, respectively. The solutions underwent a stirring at 55°C for 2 h to make them homogeneous and clear, followed by aging at room temperature for 24 h. The resulting solutions were deposited at 2500 rpm for 30 s. After each coating, the films were preheated at 250°C for 10 min. Finally, these films were annealed at 500°C for 1 h.

Structural and morphological properties of the films were analyzed using X-ray diffraction (XRD) with Cu-Kα line ($\lambda = 0.154$ nm) and atomic force microscopy (AFM) with tapping mode. The optical properties were obtained by transmission spectra [ultraviolet–visible (UV–vis) in 350–800 nm region], photoluminescence spectroscopy (using a 325 nm xenon lamp as excitation source) and Raman spectra (with 514 nm excitation laser). The photocurrent measurements were performed in an electrochemical cell using a UV light of 365 nm.

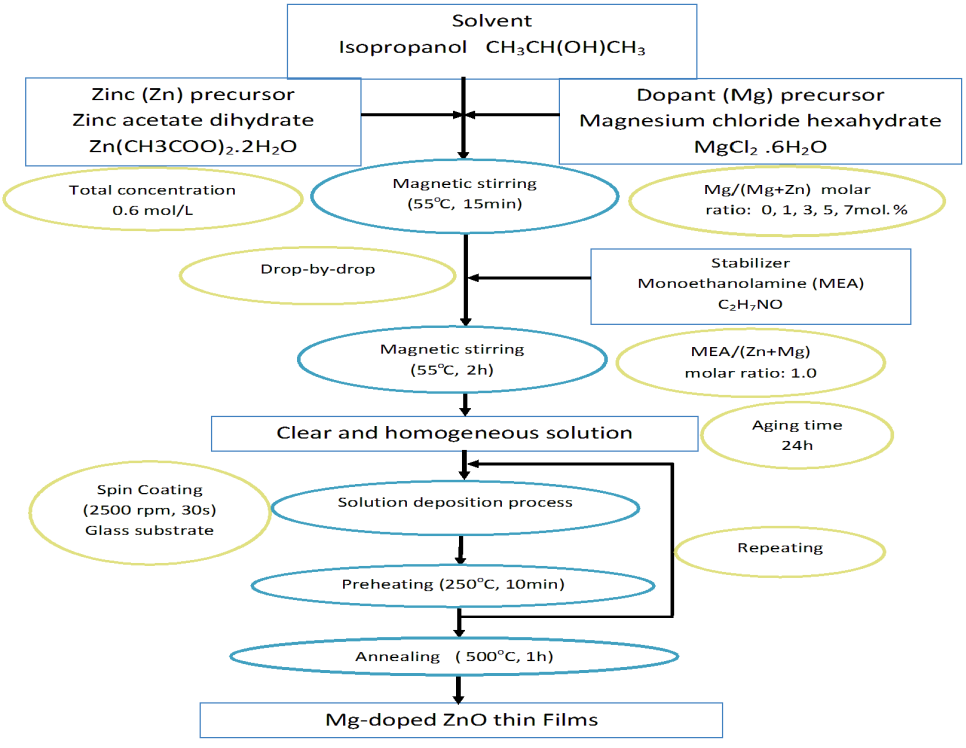

Fig. 1. (Color online) Flowchart of sol–gel process for preparing Mg-doped ZnO nanostructured thin films.

3. Results and Discussion

3.1. *Structure and surface morphology of Mg-doped ZnO thin films*

The effect of Mg doping on the crystal structure and preferred orientations of the obtained films was analyzed by the XRD technique. XRD patterns of ZnO films with Mg doping concentrations of 0, 1, 3, 5 and 7 mol.% are shown in Fig. 2. All the films exhibited a good crystallinity with a strong peak, which corresponded to the (002) plane of the wurtzite structure of ZnO (JCPDS file No. 36-1451), indicating the high c-axis growth-preferred orientation of ZnO grains perpendicular to the substrate.[24] The inset (a) of Fig. 2 shows the variations of position and intensity of the (002) diffraction. It can be seen that the intensity of the (002) peak of ZnO is enhanced significantly with increasing the Mg dopant concentration, which confirmed the improvement of the crystalline quality and the reduction of defects in the crystal structure. The diffraction peak was shifted towards higher diffraction angles as Mg dopant concentration was increased, which was due to the fact that the Mg^{2+} ions with smaller radius replaced the Zn^{2+} ions with larger radius. Replacement of Mg in the Zn site reduces the interplanar spacing $d_{(002)}$ [see inset (b) of Fig. 2], which induces this type of angle shift.[12,13,15,30] In addition, no peak corresponding to the secondary phase is observed, which confirms that the Mg^{2+} is well incorporated into the ZnO host lattice. The crystallite size was calculated from the (002) peak of ZnO:Mg films for different Mg concentrations using the Debye–Scherrer formula[15]: $D = K\lambda/\beta\cos\theta$, where D is the crystallite size, λ is the X-ray wavelength, K is a constant of 0.9, θ is the diffraction angle and β is the full-width at half-maximum. As seen from the inset (b) of Fig. 2, the crystallite size of Mg-doped ZnO thin films slightly decreased with increasing the Mg concentrations, where the presence of Mg ions prevented the growth of crystallite. Similar results were reported by Arshad *et al.*[23] Also, an atomic force microscope was used to study and measure the surface roughness and average grain size of the films of $1 \times 1\,\mu m^2$ area by tapping mode. AFM (2D and 3D) images of the surface morphologies of films are shown in Fig. 3. The surface morphology was found to be influenced by the incorporation of Mg. Small grains in the film were observed and their size gradually became smaller when the Mg ratio increased. Thus, the Mg atoms would increase the density of nuclei and prevent grain growth which in turn decreases the grain size. Moreover, similar trend has been observed for XRD results. As listed under AFM images, the root mean square roughness decreased when the Mg content increased, which was possibly related to the decrease of the average grain size by incorporation of the Mg dopant.

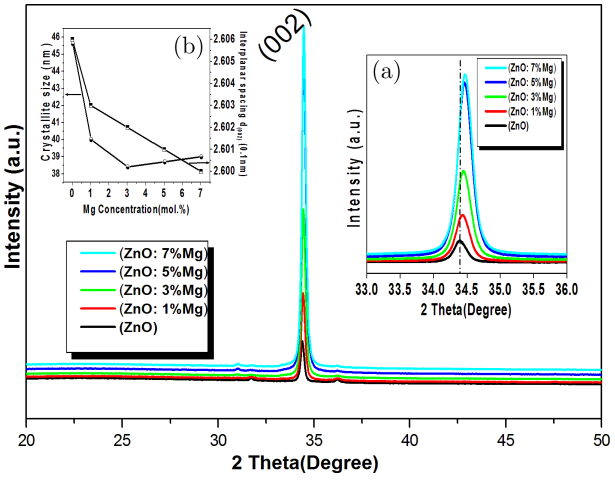

Fig. 2. (Color online) XRD patterns of undoped and Mg-doped ZnO thin films.

3.2. *Optical properties of Mg-doped ZnO thin films*

Ultraviolet–visible, Raman and PL spectroscopies are powerful methods for studying the optical properties and luminescence of ZnO thin films. The transmittance spectra of thin films are shown in Fig. 4. All films have an average transmittance above 90% in the visible region and present sharp ultraviolet absorption edges in the UV region. Furthermore, a blueshift of the absorption edges can be observed with increasing Mg doping. To evaluate the bandgap energy (E_g) from the optical absorption spectra, $(\alpha h\nu) = A(h\nu - E_g)^n$ relationship[14] is employed, where α is the absorption coefficient, A is a constant, $h\nu$ is the photoenergy, E_g is the optical bandgap and n is taken as 1/2 for direct bandgap semiconductors. The bandgap is then evaluated by extrapolating the linear region of $(\alpha h\nu)^2$ versus the photon energy. It can be seen from Fig. 5 that the optical bandgap energy increases from 3.26 eV to 3.33 eV with increasing the Mg concentration, which confirms that

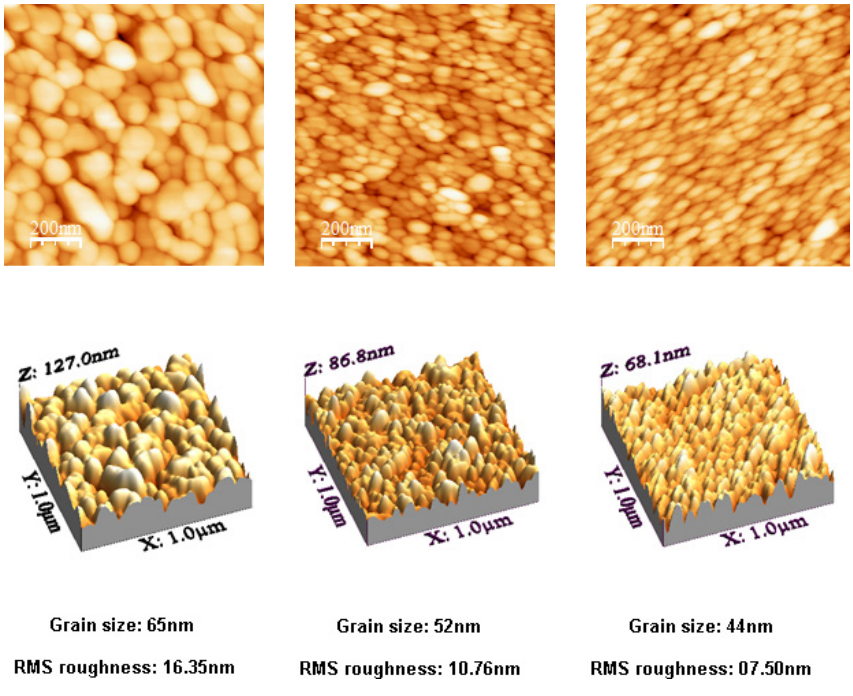

Fig. 3. (Color online) Tapping-mode AFM images (2D and 3D) of surface morphologies ($1 \times 1\,\mu m^2$) of (a) undoped ZnO, (b) doped ZnO with 3 mol.% Mg and (c) doped ZnO with 5 mol.% Mg.

the Mg ions have been incorporated into the ZnO host lattice. Similar results are also reported by Huang *et al.*[14] and Yusuf *et al.*[16] The blueshift of the absorption edge and the increase in optical bandgap with the Mg concentration, in particular the great shift for 7 mol.% Mg-doped ZnO sample, may be due to the improvement of the crystalline quality and decreasing of the crystallite size by Mg doping, or due to the higher bandgap of MgO.[12,26] Other research groups[25,29] reported that absorption edge shifting and the blueshift of ultraviolet emission peak can be attributed to the Burstein–Moss effect.

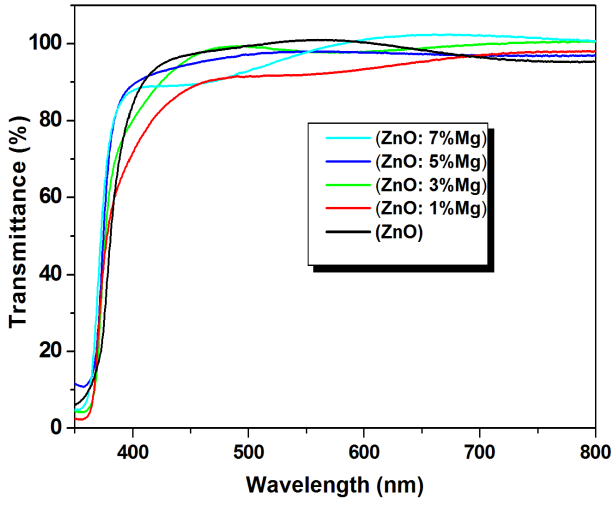

Fig. 4. (Color online) Transmittance spectra of Mg-doped ZnO thin films.

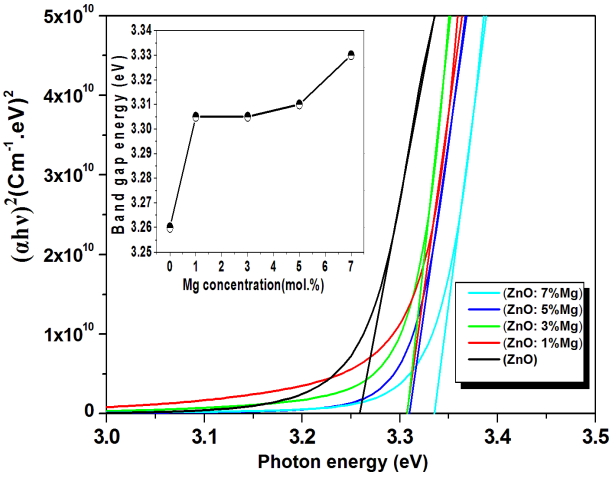

Fig. 5. (Color online) The plots of $(\alpha h\nu)^2$ versus photon energy ($h\nu$) of undoped and Mg-doped ZnO thin films and their bandgaps.

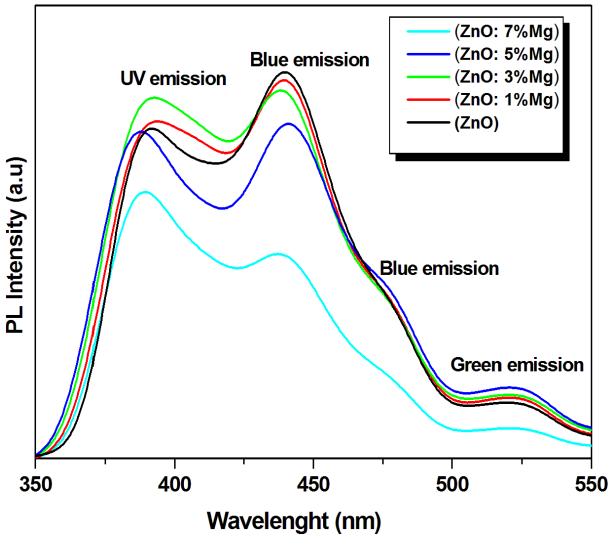

Fig. 6. (Color online) The PL spectra of undoped and Mg-doped ZnO thin films.

Figure 6 shows the PL spectra at room temperature of the Mg-doped ZnO thin films for various Mg concentrations. The PL emission spectra for all the samples were measured in the wavelength range of 350–550 nm. Generally, the PL of ZnO exhibited one emission peak in the UV region attributed to exciton recombination and more emission peaks in the visible region. The latter is due to donor defect states such as Zn interstitials (Zn_i), oxygen vacancies (V_O), acceptor defect states such as zinc vacancies (V_{Zn}) and oxygen interstitials (O_i).[30] The intensity ratio of UV peak to visible peak is mainly influenced by the crystal quality of the films as the density of defects in films decreases with an enhancement of the crystallinity. All our films exhibited a UV emission in the range of 385–388 nm corresponding to the near-band edge transition (NBE) of ZnO[14,19] and three other visible emission peaks observed at 440, 479 and 522 nm, which corresponded to the blue and green emissions. Xu *et al.*[31,32] calculated various defect state positions of ZnO thin films, and reported that the green emission was attributed to O_i and O_{Zn} defects, while the blue emission was assigned to Zn_i. The blue emission peak observed at about 440 nm can be ascribed to the transition energy of an electron from Zn_i to the valence band[33,34] and the other blue emission, which is around 479 nm, may result from the transition between the ionized oxygen vacancies and the valence band.[34,35] The green emission peak at 522 nm can be assigned to the transition energy from the conduction band to the O_{Zn} level.[32–36] Wang *et al.*[37] reported that the blue emission peak at 445 nm, the broad emission band centered at 470 nm and the green region around 510 nm are due to the emissions of interstitial zinc, singly-ionized oxygen vacancies and oxygen vacancies, respectively. Mahamuni *et al.*[38] reported that the blue–green emission may result from the electron transition from the oxygen vacancies to the interstitial oxygen. In our study, we also noted that the emission intensity ratio of UV to visible (I_{UV}/I_{vis}) increases in relation to Mg concentration, which is attributed to decreasing the defects concentration and improving crystal quality.

The wurtzite structure ZnO possesses six Raman-active optical phonons,[34] namely $E_{2L} + E_{2H} + A_{1T} + A_{1L} + E_{1T} + E_{1L}$. E_{2L} (low) and E_{2H} (high) modes were assigned to the vibrations of zinc sublattice and oxygen atoms, respectively. The room-temperature Raman spectra of undoped and Mg-doped ZnO thin films are shown in Fig. 7. Two Raman modes were observed at 99 cm^{-1} and 437 cm^{-1}, respectively. These modes were assigned to E_{2L} and E_{2H} modes, respectively, for the ZnO wurtzite structure.[4,34] The presence of E_{2L} and E_{2H} and the absence of any optical modes of other phases prove a good crystalline quality of the films. We concluded that the structural and optical properties of ZnO thin films were successfully improved by Mg doping.

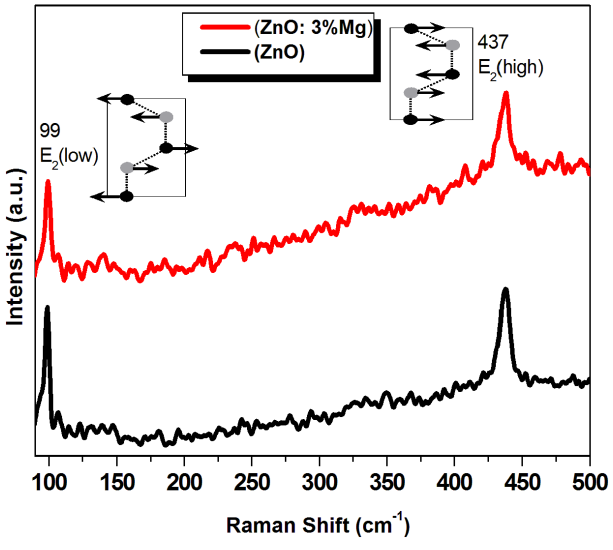

Fig. 7. (Color online) Raman spectra of undoped and Mg-doped ZnO thin films.

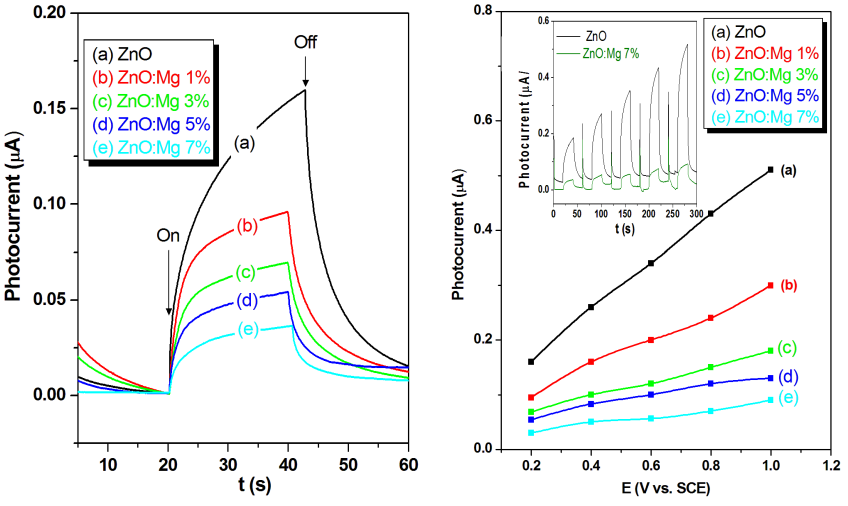

(a) (b)

Fig. 8. (Color online) (a) Photocurrents of undoped and Mg-doped ZnO thin films at a constant potential (+0.2 V) and under UV light irradiation (365 nm). (b) Photocurrent amplitude versus the applied potential for the same samples.

3.3. *UV photodetection and photocurrent studies*

Figure 8(a) shows the photoresponses of the ZnO:Mg thin films obtained by a chronoamperometric method under intermittent illumination with a 365 nm wavelength light. The photocurrent curve has an almost rectangular response under light illumination with a significant increase of current. This is due to the increase of electrical conductivity of semiconductor material, by generating of electron–hole pair, when light with energy greater than the bandgap energy is absorbed.[39] The results of photocurrent measurements versus the applied potential are shown in Fig. 8(b). Undoped ZnO thin films illuminated by a UV light source showed a pronounced photocurrent starting from 0.16 μA at 0.2 V and increased to reach 0.52 μA at 1.0 V, whereas Mg-doped ZnO thin films exhibited a significant decrease in photoresponse as the doping concentration increased as shown in Figs. 8(a) and 8(b). The n-type conduction of ZnO is due to the oxygen vacancy and/or interstitial zinc defects. Therefore, the decrease in photocurrent can be explained by the decrease of these donor defects and electron density caused by Mg doping.[17,18]

4. Conclusions

Undoped and Mg-doped ZnO thin films were prepared using a sol–gel spin coating method. XRD patterns revealed that all films showed a high c-axis orientation, along the (002) plane, and the intensity of the (002) diffraction peak increased when the Mg doping concentration was increased, with a maximum crystallite size of about 46 nm for undoped films. AFM studies revealed that the grain size and the surface roughness were reduced due to the incorporation of Mg. Optical analysis exhibit that the transmittance of thin films is above 90% in the visible region, and the Mg doping significantly enhances the bandgap energy of ZnO. Photoluminescence of the films showed ultraviolet and visible emissions, and the intensity ratio of UV emission to the visible emission increased with increasing the Mg concentration. Two Raman modes assigned to E_{2L} and E_{2H} of the ZnO wurtzite structure were observed for all samples. All films presented photoresponses and a significant decrease in photocurrent was observed with increasing Mg doping.

References

1. Ü. Özgür, Ya. I. Alivov, C. Liu, A. Teke, M. A. Reshchikov, S. Doğan, V. Avrutin, S. J. Cho and H. Morkoç, *J. Appl. Phys.* **98** (2005) 041301.
2. J. Y. Hou, Z. Mei and X. Du, *J. Phys. D, Appl. Phys.* **47** (2014) 283001.
3. C. Y. Wang, S. Y. Ma, F. M. Li, Y. Chen, X. L. Xu, T. Wang, F. C. Yang, Q. Zhao, J. Liu, X. L. Zhang, X. B. Li, X. H. Yang and J. Zhu, *Mater. Sci. Semicond. Process.* **17** (2014) 27.

4. A. Mahroug, S. Boudjadar, S. Hamrit and L. Guerbous, *Mater. Lett.* **134** (2014) 248.
5. R. Vettumperumal, S. Kalyanaraman and R. Thangavel, *Mater. Chem. Phys.* **145** (2014) 237.
6. C. Abeda, C. Bouzidi, H. Elhouichet, B. Gelloz and M. Ferid, *Appl. Surf. Sci.* **349** (2015) 855.
7. K. Vijayalakshmi, A. Renitta and K. Karthick, *Ceram. Int.* **40** (2014) 6171.
8. A. J. Kulandaisamy, J. R. Reddy, P. Srinivasan, K. J. Babu, G. K. Mani, P. Shankar and J. B. B. Rayappan, *J. Alloys Compd.* **688** (2016) 422.
9. A. Das, P. G. Roy, A. Dutta, S. Sen, P. Pramanik, D. Das, A. Banerjee and A. Bhattacharyya, *Mater. Sci. Semicond. Process.* **54** (2016) 36.
10. W. Chebil, M. A. Boukadhaba, I. Madhi, A. Fouzri, A. Lusson, C. Vilar and V. Sallet, *Physica B* **505** (2017) 9.
11. P. Giri and P. Chakrabarti, *Superlattices Microstruct.* **93** (2016) 248.
12. S. H. Jeong, J. H. Park and B. T. Lee, *J. Alloys Compd.* **617** (2014) 180.
13. S. A. Azzez, Z. Hassan, J. J. Hassan, R. Perumal, A. M. Selman and M. Bououdina, *Optik* **127** (2016) 9250.
14. K. Huang, Z. Tang, L. Zhang, J. Yu, J. Lv, X. Liu and F. Liu, *Appl. Surf. Sci.* **258** (2012) 3710.
15. K. Karthick and K. Vijayalakshmi, *Superlattices Microstruct.* **67** (2014) 172.
16. G. T. Yusuf, H. O. Efunwole, M. A. Raimi, O. E. Alaje and A. K. Kazeem, *J. Nucl. Phys., Mater. Sci. Radiat. Appl.* **2** (2014) 73.
17. S. Fujihara, C. Sasaki and T. Kimura, *J. Eur. Ceram. Soc.* **21** (2001) 2109.
18. G. H. Kim, W. H. Jeong, B. D. Ahn, H. S. Shin, H. Kim, H. J. Kim, M. K. Ryu, K. B. Park, J. B. Seon and S. Y. Lee, *Appl. Phys. Lett.* **96** (2010) 163506.
19. C. Zhang, Y. Chen, S. Liu and Y. Wang, in *Proc. 2011 Symp. Photonics and Optoelectronics (SOPO 2011)* (IEEE, 2011), pp. 33–36.
20. J. Sengupta, A. Ahmed and R. Labar, *Mater. Lett.* **109** (2013) 265.
21. L. Xu, J. Su, Y. Chen, G. Zheng, S. Pei, T. Sun, J. Wang and M. Lai, *J. Alloys Compd.* **548** (2013) 7.
22. K. Ogata, K. Koike, T. Tanite, T. Komuro, F. Yan, S. Sasa, M. Inoue and M. Yano, *J. Cryst. Growth* **251** (2003) 623.
23. M. Arshad, M. M. Ansari, A. S. Ahmed, P. Tripathi, S. S. Z. Ashraf, A. H. Naqvi and A. Azam, *J. Lumin.* **161** (2015) 275.
24. P. Madahi, N. Shahtahmasebi, A. Kompany, M. Mashreghi, M. M. Bagheri-Mohagheghi and A. Hosseini, *Phys. Scr.* **84** (2011) 035801.
25. M. N. Mia, M. F. Pervez, M. K. Hossain, M. R. Rahman, M. J. Uddin, M. A. Al Mashud, H. K. Ghosh and M. Hoq, *Results Phys.* **7** (2017) 2683.
26. M. Rouchdi, E. Salmani, B. Fares, N. Hassanain and A. Mzerd, *Results Phys.* **7** (2017) 620.
27. W. Yu, X. Chen, W. Mei, C. S. Chen and Y. Tsang, *Appl. Surf. Sci.* **400** (2017) 129.
28. C. S. Chen, W. Yu, T. Liu, S. Cao and Y. Tsang, *Sol. Energy Mater. Sol. Cells* **160** (2017) 43.
29. C. S. Chen, X. D. Xie, S. Y. Cao, T. G. Liu, Y. H. Tsang, Y. Xiao, Q. C. Liu, X. F. Yang and L. Gong, *Phys. Scr.* **90** (2015) 025806.
30. D. Fang, K. Lin, T. Xue, C. Cui, X. Chen, P. Yao and H. Li, *J. Alloys Compd.* **589** (2014) 346.
31. P. S. Xu, Y. M. Sun, C. S. Shi, F. Q. Xu and H. B. Pan, *Nucl. Instrum. Methods Phys. Res. B* **199** (2003) 286.
32. P. S. Xu, Y. M. Sun, C. S. Shi, F. Q. Xu and H. B. Pan, *Sci. China A, Math. Phys. Astron.* **44** (2001) 1174.
33. H. Chen, J. Ding and S. Ma, *Physica E* **42** (2010) 1487.
34. A. Mahroug, S. Boudjadar, S. Hamrit and L. Guerbous, *J. Mater. Sci., Mater. Electron.* **25** (2014) 4967.
35. R. Elilarassi and G. Chandrasekaran, *Mater. Sci. Semicond. Process.* **14** (2011) 179.
36. N. S. Sabri, A. K. Yahya and M. K. Talari, *J. Lumin.* **132** (2012) 1735.
37. Y. Wang, X. Zhao, L. Duan, F. Wang, H. Niu, W. Guo and A. Ali, *Mater. Sci. Semicond. Process.* **29** (2015) 372.
38. S. Mahamuni, K. Borgohain, B. S. Bendre, V. J. Leppert and S. H. Risbud, *J. Appl. Phys.* **85** (1999) 2861.
39. A. Henni, A. Merrouche, L. Telli, A. Azizi and R. Nechache, *Mater. Sci. Semicond. Process.* **31** (2015) 380.